SHOCK, Vol. 46, Supplement 1, pp. 167–176, 2016

OPEN

QUANTITATIVE MRI AND DTI ABNORMALITIES DURING THE ACUTE PERIOD FOLLOWING CCI IN THE FERRET

Elizabeth B. Hutchinson,[*‡] Susan C. Schwerin,[†‡] Kryslaine L. Radomski,[†‡] Mustafa O. Irfanoglu,[*‡] Sharon L. Juliano,[†] and Carlo M. Pierpaoli[*]

[*]Eunice Kennedy Shriver National Institute of Child Health and Human Development, National Institutes of Health, Bethesda, Maryland; [†]Department of Anatomy, Physiology and Genetics, Uniformed Services University of the Health Sciences, Bethesda, Maryland; and [‡]The Henry M. Jackson Foundation for the Advancement of Military Medicine, Inc, Bethesda, Maryland

Received 8 Mar 2016; first review completed 30 Mar 2016; accepted in final form 18 May 2016

ABSTRACT—During the acute time period following traumatic brain injury (TBI), noninvasive brain imaging tools such as magnetic resonance imaging (MRI) can provide important information about the clinical and pathological features of the injury and may help predict long-term outcomes. In addition to standard imaging approaches, several quantitative MRI techniques including relaxometry and diffusion MRI have been identified as promising reporters of cellular alterations after TBI and may provide greater sensitivity and specificity for identifying brain abnormalities especially in mild TBI. However, for these imaging tools to be useful, it is crucial to define their relationship with the neurophysiological response to brain injury. Recently, a model of controlled cortical impact (CCI) has been developed in the ferret which has many advantages compared with rodent models (e.g., gyrencephalic cortex and high white matter volume). The objective of this study was to evaluate quantitative MRI metrics in the ferret CCI model, including T2 values and diffusion tensor imaging (DTI) metrics, during the acute time period. Longitudinal quantitative comparisons of *in vivo* MRI and DTI metrics were evaluated to identify abnormalities and characterize their spatial patterns in the ferret brain. *Ex vivo* MRI and DTI maps were then compared with histological staining for glial and neuronal abnormalities. The main findings of this article describe T2, diffusivity, and anisotropy markers of tissue change during the acute time period following mild TBI, and ex vivo analyses suggest that MRI and DTI markers are sensitive to subtle cellular alterations in this model. This was confirmed by comparison with immunohistochemistry, also showing altered markers in regions of MRI and DTI change.

KEYWORDS—Anisotropy, diffusion tensor imaging, microgliosis, T2 relaxometry, traumatic axonal injury

INTRODUCTION

The hours and days following traumatic brain injury (TBI) entail a crucial period for injury, protection, and repair accompanied by a complicated collection of cellular and physiological changes that can vary greatly across patients and injury types. Noninvasive imaging techniques have become important tools for both clinical diagnosis and research by enabling visualization of the location, extent, and nature of neuroanatomical and pathological changes due to brain injury. Magnetic resonance imaging (MRI) provides different modalities that provide complementary information about changes in the brain parenchymal tissue. For example, high-resolution T1-weighted imaging may provide volumetric and morphological details, whereas T2-weighted imaging is sensitive to chemical environment changes that accompany edema and hemorrhage. Quantitative MRI approaches (e.g., T2 mapping, cerebral blood flow MRI, susceptibility weighted imaging, diffusion MRI, etc.) provide specific metrics that may be used to differentiate various features of the tissue response to brain trauma. Diffusion MRI is a quantitative approach that models water diffusion to probe the structural microenvironment and may be particularly relevant for TBI studies, especially identification of white matter abnormalities, which accompany traumatic axonal injury (TAI), physiological changes such as edema, and alterations of cellularity or cell morphology.

Although MRI in the clinical and human research setting has become a commonly used and powerful approach to detect and define brain injury (1–4), the use of imaging in animal models of TBI is less common. However, with increased availability of preclinical MRI scanners and improvements in image quality, MRI methods are becoming more widely used as outcome measures to detect and monitor changes following experimental TBI in animal models (5–13). Quantitative MRI studies in rodents have demonstrated several promising avenues for investigation including T2 imaging, blood flow imaging, and diffusion MRI. Although MRI markers in these models may provide insight for understanding the pathology and trajectory of abnormalities that follow experimental TBI, it is important to understand the relevance of these models and markers for human TBI. These and other rodent studies are valuable for understanding the meaning of MRI markers that follow brain injury; however, the low relative volume of white matter and simple geometry of the rodent brain also limit them. Addressing

Address reprint requests to Elizabeth B. Hutchinson, PhD, Eunice Kennedy Shriver National Institute of Child Health and Human Development, National Institutes of Health, Bldg. 13, Room 3W16, 13 South Drive, Bethesda, MD 20892-5772. E-mail: elizabeth.hutchinson@nih.gov

Congressionally Directed Medical Research Programs Award Number: W81XWH-13-2-0019 | Recipient: Carlo Pierpaoli, MD, PhD, and W81XWH-13-2-0018 | Recipient: Sharon Juliano, PhD.

The authors report no conflicts of interest.

Supplemental digital content is available for this article. Direct URL citation appears in the printed text and is provided in the HTML and PDF versions of this article on the journal's Web site (www.shockjournal.com).

DOI: 10.1097/SHK.0000000000000659

this challenge by identifying MRI abnormalities in an animal model that more closely mimics the human brain may improve the ability to bridge observations of experimental MRI markers with human outcomes.

The objective of the current study is to evaluate the presence, nature, and extent of quantitative T2 and diffusion MRI abnormalities in a ferret model of mild controlled cortical impact (CCI) during the acute phase. The ferret was selected as the animal model of choice based on the geometric similarities of human and ferret brain, both of which are gyrencephalic and have greater relative white matter volume than rodents (Fig. 1). The CCI model was selected for its high reproducibility, and a mild severity was chosen based on the high incidence of mild TBI in human populations. A battery of MRI scans including anatomical T2-weighted imaging, T2 mapping, and diffusion tensor imaging (DTI) were performed before CCI and 1 day following injury to determine the changes in MRI parameters that accompany injury in this model during the acute phase. The overall goal of this study was to determine the signature of posttraumatic MRI and DTI abnormalities not only to better understand the pathophysiology of brain injury in this model, but also to evaluate the similarities with and differences from commonly observed imaging and immunohistochemical markers that accompany trauma in human patients.

METHODS

All animals were housed and treated according to the national guidelines established in the NIH guide and institutional oversight by the Uniformed Services University Animal Care and Use Committee. Adult male ferrets (6–12 months old, n = 11) were imaged before and 24 to 28 h following CCI.

Ferret CCI

Surgical procedures were performed using aseptic technique and in a sterilized operating suite. Ferrets were anesthetized using inhaled isoflurane (4%–5% induction and 2%–3% maintenance) and according to physiological monitoring for heart rate, respiration, and temperature. A detailed description of the surgical procedures may be found in Schwerin et al. (14). The CCI injury was directed to the left hemisphere somatosensory cortex using an electromagnetically controlled stereotaxic device (Impact One Stereotaxic Impactor, Leica Microsystems, Buffalo Grove, Ill) with an impactor tip diameter of 3 mm at a velocity of 5 m/s, depth of 2 mm, and dwell time of 100 ms.

In vivo ferret MRI

Each ferret was imaged using a Bruker 7T MRI system with either a 6 cm (Doty) or 8.6 cm (Bruker) quadrature volume coil for transmit and receive and ParaVision 6.0 software to acquire the raw images for T2 mapping and diffusion tensor MRI as described below.

T2-weighted imaging and T2 mapping

Acquisition—Multiple echo RARE imaging was used with TE values of 12, 36, 60, 84, 108, and 132 ms and TR = 10 s. A two-dimensional coronal acquisition was used with FOV = 48 mm × 48 mm, matrix = 96 × 96, slice thickness = 0.5 mm, number of slices = 42, nex = 1, and reps = 1.

Processing—The multiecho data at each voxel were fit in the native space of the acquisition according to the simple monoexponential relationship between the MRI signal with TE and T2 relaxation time. Maps were generated for T2 and also the proton density signal magnitude.

DTI

Acquisition—A two-dimensional EPI pulse sequence was used to acquire diffusion weighted image (DWI) volumes with TE/TR = 40/5,000 ms. Two aspects of this acquisition are worthy of mention as they are different from the most common approaches for preclinical DTI.

1. The spatial dimensions were selected to allow whole brain coverage and resampling to isotropic voxels to be used with three-dimensional analysis methods, specifically a coronal acquisition with FOV = 3.6 mm × 4.8 mm and matrix = 48 × 64 to yield 0.75 mm × 0.75 mm in-plane resolution with 48 slices of 0.5 mm slice thickness.
2. The entire EPI readout was acquired during the same TR (i.e., number of segments = 1). Although segmented EPI is commonly used in preclinical studies to reduce echo time and decrease geometric distortions, this approach is vulnerable to differences in motion between acquired segments, which may decrease the reliability of data to be used for diffusion modeling. To avert this problem, we chose to acquire a single segmentation with the following adjustments and corrections. To reduce the TE, we decreased the matrix size by reducing the in-plane resolution and by placing saturation bands around the extracranial tissue (i.e., muscle and skin of the head). To correct for geometric distortions, two repetitions for each DWI were collected with opposite phase-encode directions for use with diffeomorphic registration for Blip-Up blip-Down Diffusion Imaging (DRBUDDI) processing to correct geometric distortions (15).

The diffusion experimental design included two repetitions of 3 b = 0 images, 30 DWIs with b = 700 s/mm^2 and 30 b = 1,000 s/mm^2.

Processing—The raw DWIs were imported and preprocessed using the TORTOISE DTI pipeline (16) including motion and eddy current correction and DRBUDDI correction. The diffusion tensor was fit using the DIFFCALC module of the TORTOISE pipeline, and DTI maps for Trace of the diffusion tensor (TR), fractional anisotropy (FA), and directionally encoded color (DEC) maps (17) were generated.

Analysis and statistics

Voxelwise analysis of T2, TR, and FA values was performed to determine the presence and location of MRI and DTI abnormalities in a bias-free manner. First, a study-specific common template was generated for T2 and DTI separately as follows.

T2 template generation: Anatomical images were warped into a common space using the Advanced Normalization Tools package for diffeomorphic registration, and the resulting transformations were applied as well to the amplitude and T2 maps. The amplitude images were then averaged together to generate a baseline T2 anatomical template.

DTI template generation: The diffusion tensor image of each brain at baseline was warped in to a common space using DRTAMAS (18), and the resulting transformation was applied to the TR and FA maps for each brain, which were then averaged together to generate baseline DTI templates.

Next, brain maps from the 1-day time point were individually warped to the baseline template of each modality using either the Advanced Normalization Tools package for T2 images or DRTAMAS software for DTI data.

Using brain pairs from the same animal in the common template space, difference maps were generated by subtracting the baseline map (T2, TR, or FA) from the same map at 1 day. Difference maps were also generated between individual injured brains and the baseline template.

Region of interest (ROI) analysis was used to characterize quantitative differences in MRI and DTI metrics within the primary lesion, an ITKsnap semiautomatic segmentation algorithm was used to generate ROI masks of the lesion for each T2 and TR map in template space. Each mask was generated independently for TR and T2 using the maps from the 1-day time point. For the control ferrets and ferrets with no detectable abnormality, a spherical ROI was placed in the same anatomical region as for the CCI group. The masks generated from the 1-day T2 and TR maps were used for the baseline maps of the same animal. For FA, a single mask was generated using the ITKsnap algorithm to delineate a region of white matter within the lobe of injury using the FA template.

Next, ROI masks for the lesion were used to extract quantitative values for T2 or DTI metrics for each brain and time point. For each animal baseline and 1-day post-CCI values of T2, TR, and FA were plotted using the R statistical package xyplot tool, and analysis of variance was performed for the ROI data using the R statistical package CCI group and time point as factors. To compare values across metrics, scatter plots were made for the T2 and TR or FA value for each brain and statistical correlation of the metrics was determined using Pearson's correlation.

Tissue processing

At 24-h postsurgical procedure, each animal was deeply anesthetized by isoflurane inhalation (5% in oxygen) and euthanized with an i.p. overdose of Euthasol (50 mg/kg). Upon cessation of reflexes, ferrets were transcardially

perfused with 1 L of ice-cold phosphate-buffered saline (PBS) (pH 7.4) followed by 1 L of 4% paraformaldehyde solution in PBS (Santa Cruz Biotechnology, Dallas, Tex) containing 47.6 mg of heparin (Sigma-Aldrich, St. Louis, Mo). The brains were harvested, postfixed in 4% paraformaldehyde for 8 to 10 days, and then transferred to a storage solution containing 0.03% sodium azide in PBS (PBS-NaN_3). After *ex vivo* MRI scanning, the brains were cut at 50-μm thick coronal sections using a vibratome (Leica VT1000; Leica) and stored in PBS-NaN_3 at 4°C until use in histological processing.

Immunohistochemistry

Sections were selected for histological examination based on MRI and DTI findings. After antigen epitope retrieval with 1X Citrate buffer (Thermo Scientific, Waltham, Mass) for 20 min in a 60°C water bath, the sections were rinsed with PBS and incubated in blocking buffer solution (0.1% Triton X-100, 3% normal goat serum in PBS) for 2 h at room temperature (RT), followed by an overnight incubation with primary antibodies at 4°C. Primary antibodies used included markers for astrocytes (GFAP, 1:500, Abcam, ab4674); macrophage/microglia (Iba1, 1:1,000, Wako, 019019741); myelin oligodendrocyte glycoprotein (MOG, 1:300, Sigma, SAB1406138); and dendritic microtubule-associated protein 2 (MAP2, 1:200, Abcam, ab5392). After three PBS washes, staining was revealed by 2-h incubation at RT with the appropriate Alexa 488 or 555 conjugated secondary antibodies (Invitrogen) diluted 1:500 in blocking buffer. DAPI (4′,6-Diamidino-2-phenylindole, 1:2,000, Invitrogen, D21490) was added to the secondary antibody solution for nuclear counterstaining. Following three more washes in PBS, the sections were mounted onto slides and coverslipped with Mowiol 4-88 (Polysciences) mounting medium. Immunolabeled brain sections were then analyzed and imaged using a Zeiss Axiovert 200 microscope equipped with an Apotome and Axiovision 4.7 Zen software (Carl Zeiss, Inc, Oberkochen, Germany).

RESULTS

In this study, mild CCI resulted in several notable MRI and DTI abnormalities that were discernable in individual animals, quantitatively different within the metrics examined and localized to regions of the brain that were not directly impacted by CCI, especially the white matter. Histopathology confirmed the presence of subtle abnormalities and also highlighted the heterogeneity and multiplicity of cellular alterations that correspond to imaging markers.

Imaging abnormalities 1 day following mild CCI are discernable in individual ferret brains

In vivo abnormalities on individual images and maps were detected and discernable by eye for 7/8 ferrets assessed at 24 h following CCI. The most consistent and prominent abnormality was T2 hyperintensity and increased T2 values (Figs. 2 and 4). For several ferrets, a region with increased TR was also discernable by eye (Fig. 3A) and decreased FA in the white matter near the injury site could be visualized by comparison with the contralateral side (Fig. 3B).

Longitudinal comparison of the T2 and DTI maps within the same animal before injury and 1 day following CCI was used to assess the presence of abnormalities as well as determine the effect size and location of changes resulting from the injury. Individual T2 and DTI maps of the ferret brain 24 h following injury were also compared with a normative template generated from all baseline maps to demonstrate the utility of this type of comparison for cases when a baseline image may not be available (see Figure, Supplemental Digital Content 1, at http://links.lww.com/SHK/A400, which demonstrates the similarity of difference maps calculated by comparing individual injured brains to the baseline map of the same brain and to the template from all baseline maps). Difference maps for T2 in a single animal (Fig. 2C) showed robustly increased T2 localized to the white matter of the cortex near the injury site. Similar difference maps between imaging sessions were generated for DTI maps of TR and FA for the same ferret (Fig. 3B). These show robust increased in TR and decreased FA in the lobe of the cortex near the injury site. The spatial profile for these abnormalities is different as FA is more highly localized to the white matter, whereas the TR abnormality is more extensive. It should be pointed out that difference maps are affected by the uniformity of the underlying map and that *in vivo* values of T2 and TR are quite uniform across the brain, whereas FA is more sensitive to white matter (WM).

Ex vivo T2 and DTI abnormalities were also discernable by eye in 3/3 fixed brains that were evaluated in this study although differences between the *in vivo* and *ex vivo* markers highlight the importance of interpretation across these two approaches. T2 values were generally shorted for the whole brain in fixed tissue compared with *in vivo* and greater contrast was found between gray matter and WM (Fig. 2A). In the region of T2 hyperintensity on *in vivo* MRI, *ex vivo* T2 mapping of the same brain showed a central core of decreased T2 surrounded by

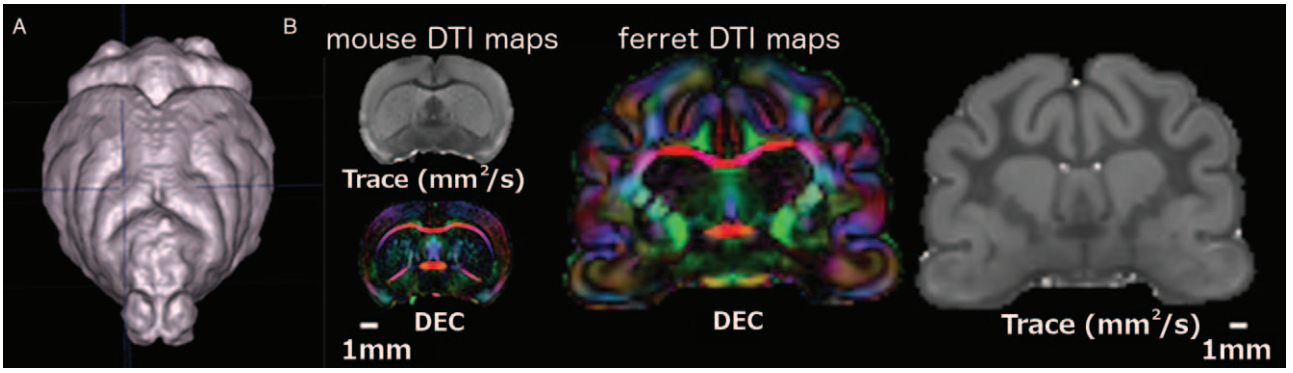

FIG. 1. ***Ex vivo* MRI and DTI maps show several important features of ferret brain.** A, The folded cortical surface and gross morphology can be seen in the three-dimensional rendering where the blue crosshairs indicate the primary somatosensory cortex, which is the site for CCI placement. B, Representative slices from DTI maps of the mouse and ferret brain are shown in the same spatial scale to demonstrate differences in geometry and white matter content. The Trace map indicates the diffusivity of water in the specimen and shows contrast between gray and white matter. The DEC map is weighted by anisotropy and indicates the primary orientation of the white matter fibers (red—L/R, blue—D/V, green—A/P), which makes clear the greater complexity of the ferret white matter compared with that of the mouse. CCI, controlled cortical impact; DEC, directionally encoded color; DTI, diffusion tensor imaging; MRI, magnetic resonance imaging.

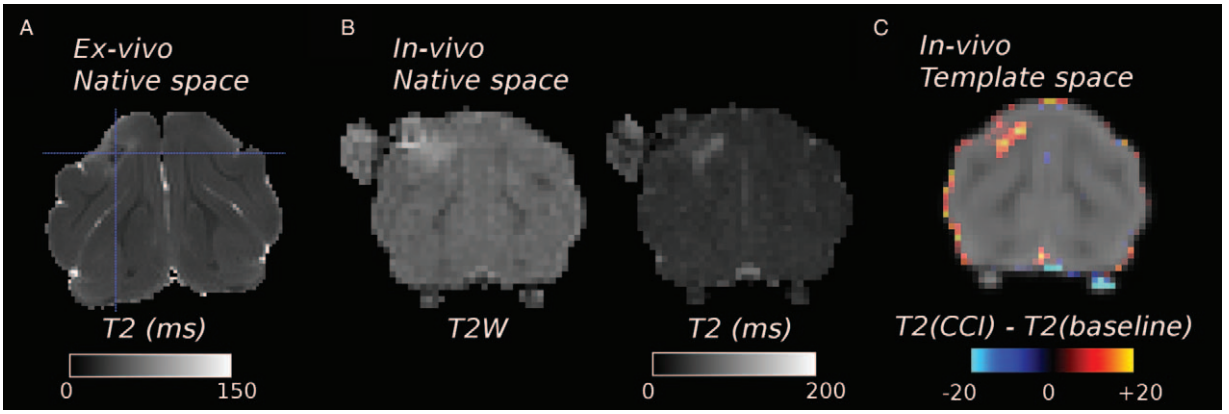

Fig. 2. **T2 MRI abnormalities are shown for the same ferret brain 1 day following CCI.** A, The *ex vivo* T2 map at the level of the CCI site shows a focal core of decreased T2 (blue crosshairs) surrounded by increased values of T2, which localize to the cortical surface near the CCI site and along the white matter of the cortex. B, *In vivo* MRI and T2 maps of the same brain show T2 hyperinstensities in a continuous region of cortex and white matter near the injury site and the T2 maps reveals the greatest values of T2 in the white matter. C, A voxelwise comparison of T2 values from *in vivo* MRI of acquired at baseline and following CCI is overlain on an MRI template generated from all baseline scans. The greatest differences in T2 are localized to the white matter of the cortex in the same lobe as the CCI site. CCI, controlled cortical impact; MRI, magnetic resonance imaging.

increased T2 that was especially localized to the white matter and the cortical surface. *Ex vivo* TR maps were perhaps the most distinct from their *in vivo* counterparts. Although *in vivo* TR values are similar in gray matter and WM, there is strong contrast between tissue types in the *ex vivo* maps. For the case shown in Figure 3C, a small region of increased diffusivity can be seen surrounded by low TR values, and in the other two *ex vivo* cases (Figs. 7 and 8) the primary *ex vivo* TR abnormality was decreased diffusivity. This abnormality is opposite to the increased TR found *in vivo* in the same tissue regions. On the contrary, FA was similarly decreased in white matter regions near injury for both *in vivo* and *ex vivo* maps (Fig. 3).

In vivo T2 and DTI metrics offer complementary information in the injured brain

Quantitative longitudinal T2, TR, and FA values within regions of abnormality are plotted for each ferret in Figure 4. The magnitude of T2 increase for all ferrets in the CCI group was similar, and for the single ferret in this group with no observed T2 abnormality, the T2 values were similar to

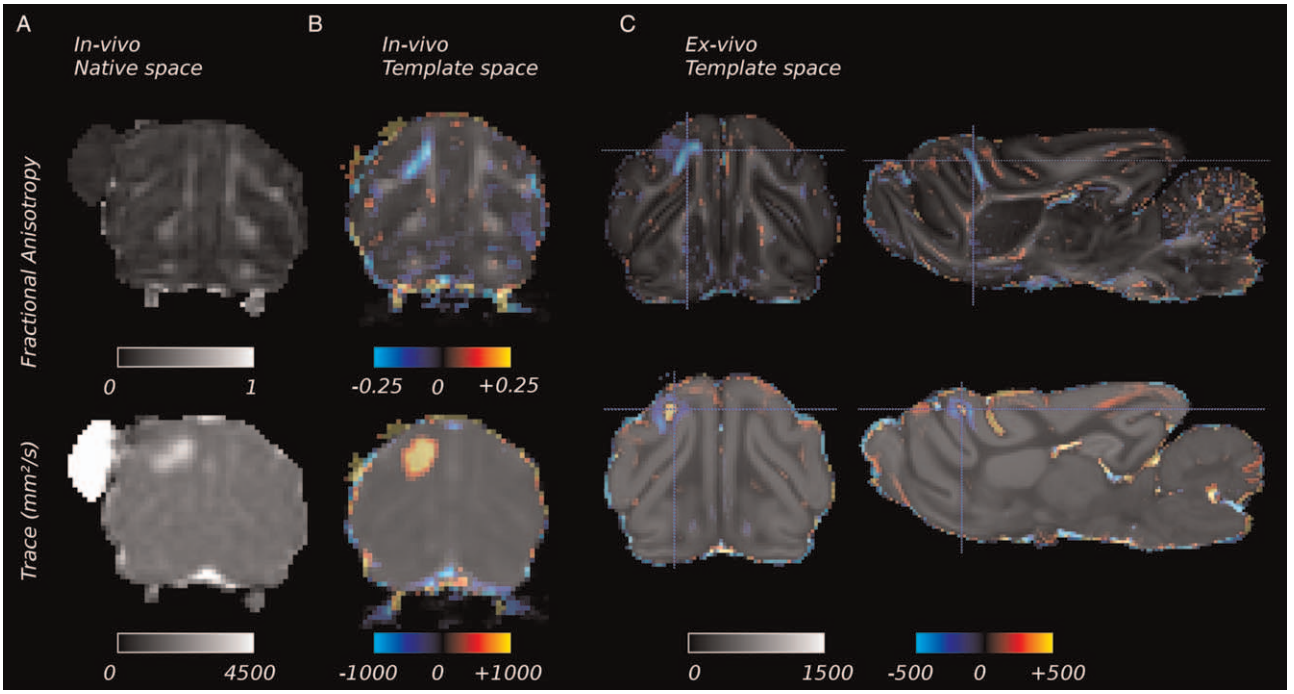

Fig. 3. **DTI abnormalities are shown for the same ferret brain as in Figure 2.** A, *In vivo* FA and TR maps show increased TR and decreased FA in a region of the cortex and cortical WM near the injury site. B, Voxelwise difference maps for this ferret of TR and FA map quantitative differences between the maps acquired 1 day after CCI and those form the baseline imaging session. The range of each colored difference map is given by the color bar and overlain on the TR and FA templates generated from all baseline DTI maps. C, A similar voxelwise analysis for the same ferret brain is shown for *ex vivo* DTI difference maps in the coronal and sagittal views where the blue crosshairs indicates the same point in both planes. CCI, controlled cortical impact; DTI, diffusion tensor imaging.

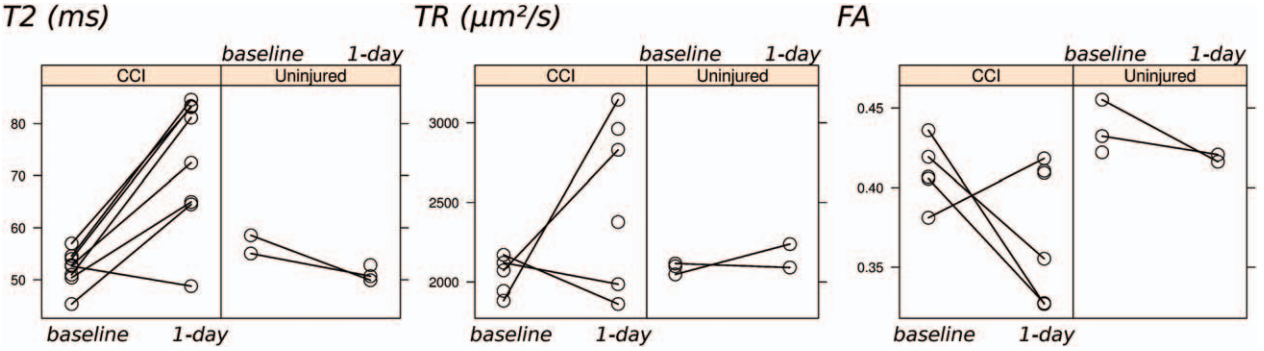

FIG. 4. **Quantitative longitudinal MRI and DTI values are plotted for each ferret from images acquired at baseline (before injury) and 1 day after CCI.** Each point represents the mean value of T2, TR, or FA within a region of interest (ROI) mask generated based on the abnormality of each type of map. For T2 and TR, ROIS were generated using the postinjury maps for each ferret and applying a semiautomated local threshold based algorithm. When no abnormality was present, an ROI placed on the template was used. For FA, the same ROI was used for all maps and was generated using the baseline FA template to delineate a portion of white matter in the cortex near the injury site. Lines in these plots join data points from the same ferret when both scans were included and the results for the uninjured and CCI model group are separated. CCI, controlled cortical impact; DTI, diffusion tensor imaging; MRI, magnetic resonance imaging.

the uninjured group at both time points. Although between-group main effects were not significant by ANOVA, there was a significant main effect of time relative to injury ($P < 0.05$) and interaction of CCI group and time relative to injury ($P < 0.005$) upon within-subject testing. The DTI metrics of TR and FA were less consistently changed for each animal than the T2 values, and ANOVA found no significant effects of interactions between groups or within subjects.

The correspondence of T2 and DTI metrics was examined by plotting the values for T2 against TR and FA, respectively, for the baseline and post-CCI maps (Fig. 5). Although a statistically significant correlation ($R^2 = 0.71$, $P < 0.05$) was found between TR and T2 values in lesioned regions following CCI, inspection of individual points demonstrate several lesions with low TR values, but increased T2 suggesting a more complicated relationship between these metrics. In particular, three points from the 1-day maps demonstrate both elevated T2 and TR, whereas two points from this group show only elevated T2. The correlation of T2 with white matter FA was significant, but low ($R^2 = -0.63$, $P = 0.03$), and as for the case of TR, inspection of the individual data points reveals patterns of complementary information between the T2 and FA metrics.

To determine the localization of imaging abnormalities, the maps for each metric were examined across all *in vivo* scans in the study by creating average difference maps for T2, TR, and FA based on the difference maps for each ferret (Fig. 6). For all three metrics, the most extensive *in vivo* abnormalities were along the white matter in the lobe of the brain near the site of injury. Evidence of white matter abnormalities was also present for the *ex vivo* maps, however not as robust as the *in vivo* maps suggesting the strong dependence of these markers on physiological alterations.

Ex vivo MRI and DTI abnormalities near the cortical surface correspond to regions of microglial alterations and a reduction of neural processes

Ex vivo DTI maps revealed regions of decreased TR and abnormal FA especially in the gray matter near to the cortical surface at the injury site (Figures 7, 8, and 9) and extending several millimeters away from the site. The comparison of DTI and immunohistochemical staining revealed several histological correlates of imaging abnormalities identified in this study. In Figure 7, located at the lesion center, a decrease in gray matter intensity in the TR image correlated with subtle changes

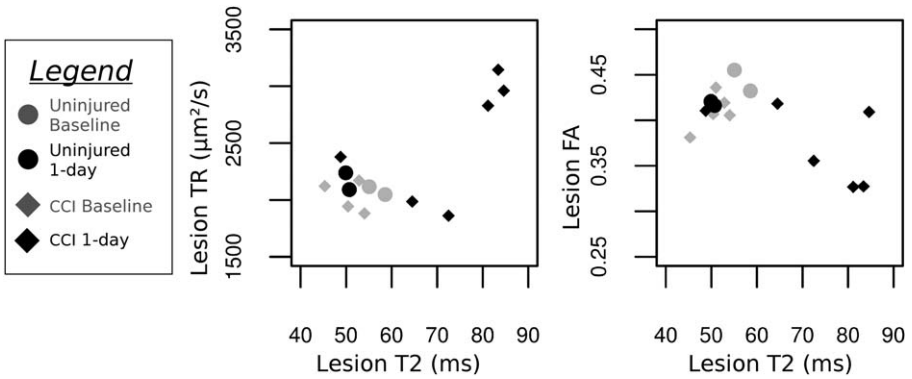

FIG. 5. **To examine the correlation of T2 and DTI values, scatterplots of ROI data from each metric are shown.** Each point corresponds to the metric values of T2 and TR or FA in the same ferret from the same imaging session. ROIs were generated as previously described in Figure 4 and black circles indicate data points from the baseline imaging sessions, whereas red circles indicate data from the sessions 1 day following CCI. CCI, controlled cortical impact; DTI, diffusion tensor imaging; ROI, region of interest.

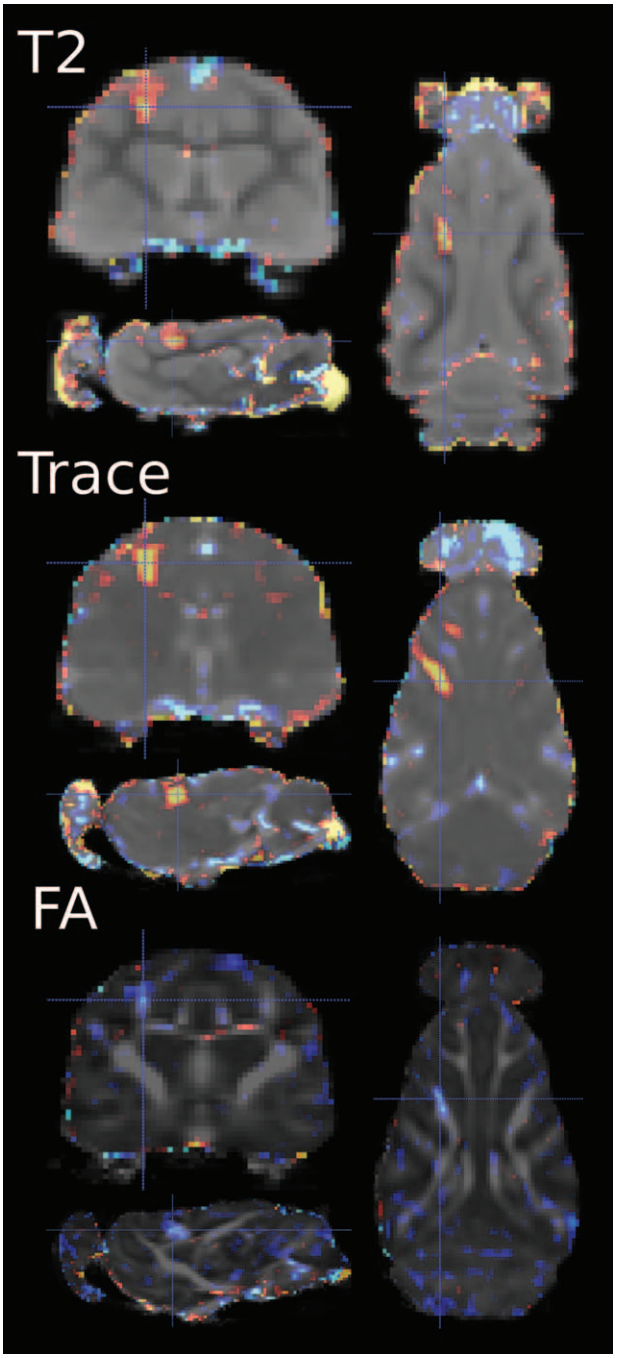

Fig. 6. **Spatial patterns of *in vivo* T2 and DTI abnormalities following CCI.** Average difference maps were generated on a voxelwise basis by the mean value the T2, TR, and FA differences generated for each ferret with a detectable individual abnormality of the given metric. The difference maps for each metric show strong localization of the imaging markers to the white matter. CCI, controlled cortical impact; DTI, diffusion tensor imaging.

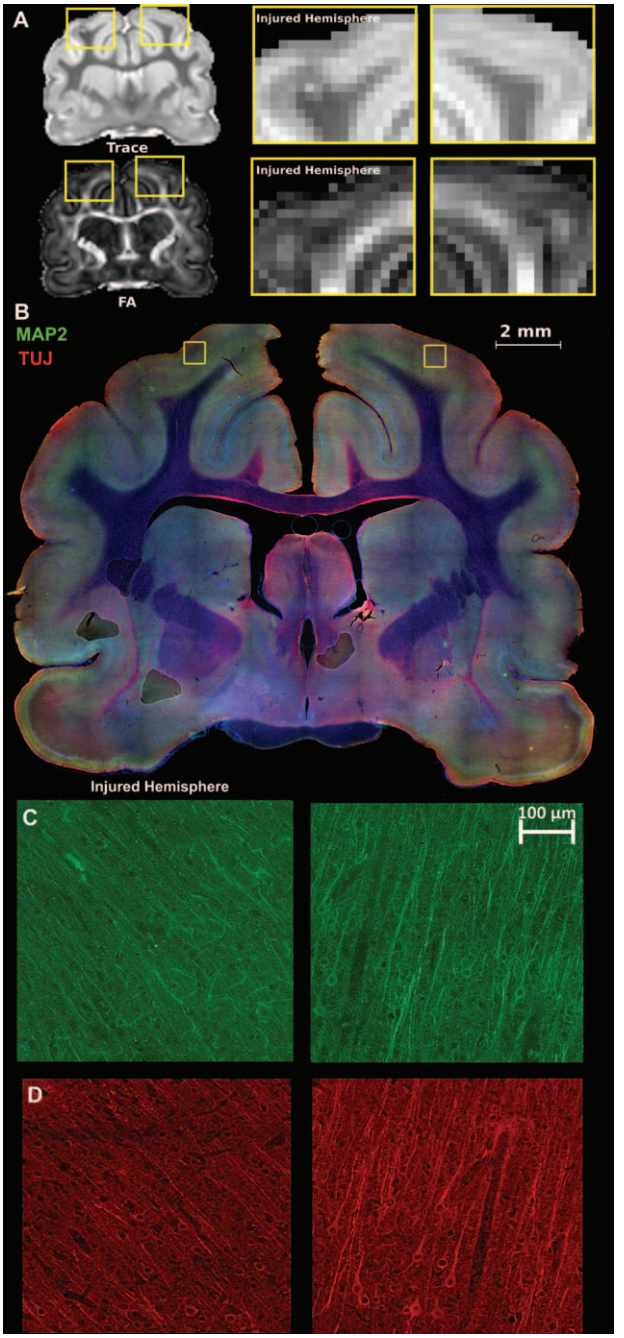

Fig. 7. ***Ex vivo* DTI markers of cortex and white matter abnormalities in a single brain taken 1 day following CCI were compared with fluorescence labeled immunohistochemistry.** A, DTI maps for Trace and FA for the whole slice at the level of CCI injury and magnified regions of the DTI maps reveal regions of decreased Trace and FA near the CCI site compared with the uninjured side. B, A low power image of the same brain showing immunoreactivity for MAP2 and Tuj1, both neuronal markers. A decrease in staining can be seen in the same region that shows abnormalities in the DTI maps. C and D, Higher power images of the site show that both MAP2 and Tuj1 indicate reduced numbers of processes. CCI, controlled cortical impact; DTI, diffusion tensor imaging.

in the immunoreactivity for Tuj1 and MAP2. Both of these markers demonstrate neuronal elements and are reduced in the cortex ipsilateral to the lesion. The injured side shows fewer processes extending through the cortical thickness for both markers. Figure 8 is anterior to the lesion core and also shows decreases in the TR images. For both brains (A and B), this anterior region of low density is more extensive than that observed in Figure 7 and corresponds to an increase in immunoreactivity for microglia (Iba1). The FA image is also altered at this site, and possibly results from changes in morphology of microglia, which are enlarged with extensive processes, compared with microglial immunoreactivity in the contralateral hemisphere. The distribution of the microglia

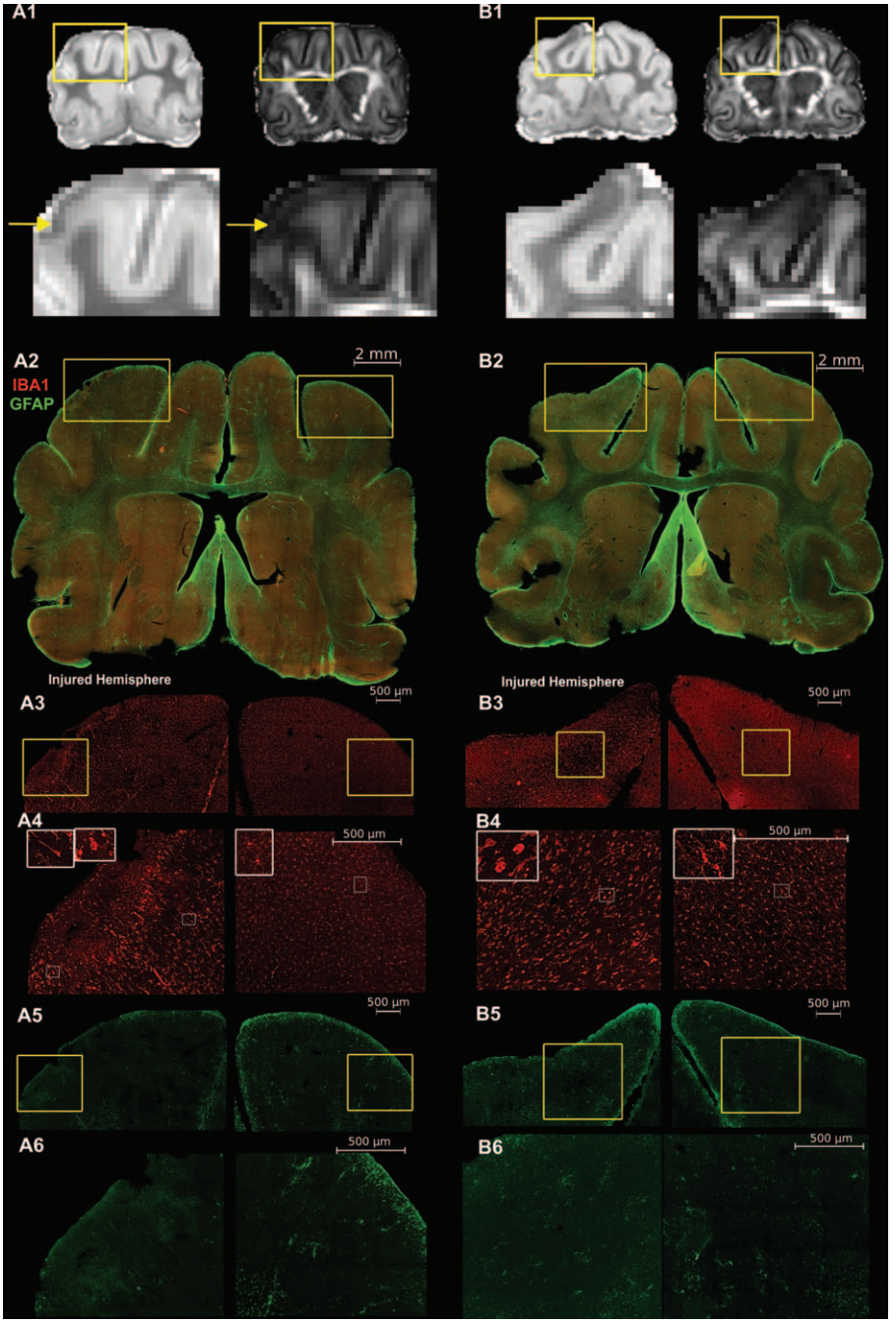

FIG. 8. **A1 and B1, Regions anterior to the lesion core also show DTI abnormalities, although subtle differences between two different brains may be appreciated.** Both brains demonstrate regions of decreased Trace in the cortical gray matter, but B1 shows decreased FA, whereas A1 shows a region of normal or increased FA. A2 and B2 are low power views of immunoreactivity for microglia (Iba1) and astrocytes (GFAP) in the same brains. Regions of altered immunoreactivity can be seen in the yellow-boxed regions. At higher power in A3–A4 and B3–B4, distinctions are evident in microglial immunoreactivity. On the side of the lesion, a pattern of altered Iba1 staining can be seen surrounding the lesion in A3–A4. The cells are hypertrophic and some are oriented. The white boxes show more magnified cells in the insets. In B3–B4, changes are also evident in the injured region, with enlarged and apparently reactive microglia. A5–A6 and B5–B6 show GFAP reactivity, which shows very little distinction between the injured and opposite hemisphere at 1-day post-TBI. The yellow-boxed regions in A5 and B5 are shown in higher power in A6 and B6. DTI, diffusion tensor imaging.

seems to follow a pattern that relates to the injury, which is also seen on the TR image. This is especially true for the example shown in Figure 8, A3–A4, whereas B3–B4 show enlarged and hypertrophic microglial cells. The immunoreactivity for astrocytes (GFAP) was minimal, and appeared at the cortical surface associated with the pia and around blood vessels in both hemispheres, as it is typical for immunoreactivity in the cerebral cortex. Figure 9 shows immunoreactivity for multiple markers that correspond with changes in MR images. GFAP, as in the previous figure, seems relatively normal, with very subtle changes in the injured cerebral cortex. The microglia, however, show altered morphology and changes in overall distribution. The immunoreactive cells on the lesioned side are hypertrophic with ramified processes, whereas the opposite side shows immunoreactive microglia with smaller soma and a more regular distribution. Immunoreactivity for myelinated

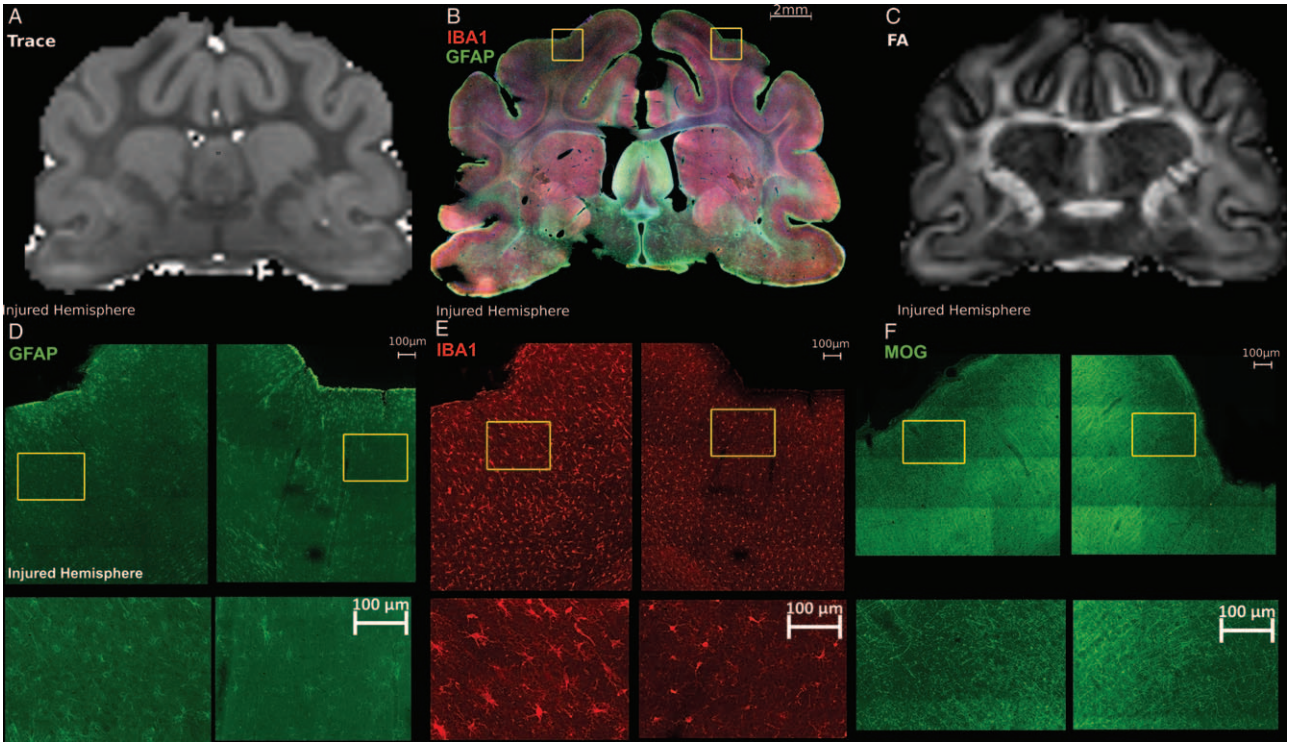

Fig. 9. **A and C, DTI maps for the Trace and FA, for which decreases in both values are present in the cortical gray matter.** B, A low power image of immunoreactivity against GFAP (astrocytes) and Iba1 (microglia). D, The astrocytic changes at 1-day post-TBI are subtle and show only slight alteration. The microglia shown in (E) are enlarged, with extensive processes and appear reactive on the injured side, whereas those in the opposite hemisphere are smaller with minimal processes. The myelin (MOG) staining in (F) reveals a decreased number of fibers, especially in the upper layers. The boxes in (D–F) are shown at higher power in the lower set of images. DTI, diffusion tensor imaging.

processes (MOG) also corresponds to changes in the TR and FA, showing decreases in myelinated fibers, especially in the upper layers of the neocortex.

DISCUSSION

Following mild TBI in the ferret, several *in vivo* MRI markers were discernable by eye in individual T2 and DTI maps and quantitatively robust by ROI and voxelwise comparisons to baseline values from the same brain or using a normative template of all baseline maps. Within these markers, differences emerged, especially between T2 and TR, that highlight the complementary information that may be obtained using these methods in combination and indicate potential pathophysiological mechanisms in the model. In addition to identification of quantitative changes in MRI values, T2 and DTI abnormalities were found to be localized preferentially in the white matter. Finally, the comparison of DTI markers in fixed tissue with histology in the same brain regions demonstrates the complexity and heterogeneity of the cellular alterations that underlie the observed imaging abnormalities.

The recent development of the CCI model in the ferret (14) is an important contribution to understanding the nature of brain injury outcomes that mimic what is found in humans. In particular, the gyrencephailc cortex of the ferret and high relative white matter are distinctly more similar to the human brain than the lissencephalic geometry and low relative white matter of the rodent brain. In this study, the mild CCI injury did not directly impinge on the white matter, but resulted in robust changes in the white matter T2, TR, and FA values. This is consistent with several commonly observed MRI features of human TBI including T2-weighted imaging which is a primary MRI approach for detecting edema and hemorrhage and also sensitive to TAI in the white matter during the acute period (2). Diffusion imaging in human studies has determined the presence of diffusivity and anisotropy abnormalities (19–21) in the white matter during the acute period that are associated with TAI. The strong localization to white matter of T2 and diffusion abnormalities in this study of the ferret demonstrate a similarity to the predominance and imaging features of white matter abnormalities in human studies as well as suggest that the ferret provides a suitable model to study focal TAI.

The combination of T2 and diffusion markers of injury to describe pathophysiology in TBI logically follows the well-established use of these methods to characterize ischemic stoke (22), and the commonalities and differences among MRI markers in these distinct disorders may offer clues to the role played by ischemia in TBI. Experimental and clinical stroke studies have determined that only minutes following vascular occlusion diffusivity is decreased, but T2 is normal and increases hours and days later with the appearance of vasogenic edema. The acute decrease in diffusivity returns to normal values several days after injury, and the initially expansive T2 abnormalities ultimately resolve in extent although some regional abnormalities may persist. In the current study, all ferrets exhibited a region of increased T2 following CCI, but only a subset of these animals showed clear diffusion abnormality. Furthermore, unlike for ischemic stroke, the

predominant diffusion change was to increased TR. This MRI distinction from the traditional markers of stroke is an important indication about the potential underlying pathophysiology in this model. A relevant previous study of T2 and diffusivity (23) in an experimental model of microvascular infarct with early vasogenic edema demonstrated several regions of increased diffusivity and increased T2 for which the most robust increases in diffusivity were localized to the white matter and correlated with electron microscopic evidence for spreading extracellular edema. This suggests that for the cases of increased T2 and increased TR in this study, there is extracellular edema between the fibers of the white matter. Importantly, this also implies that the white matter in these cases is not metabolically compromised as this would lead to reduced TR similar to stroke due to cytotoxic edema. This second scenario of damaged white matter is a possible interpretation in two cases from this study for which T2 was elevated in the absence of TR changes, although healthy white matter with minimal edema would also explain this finding. In gray matter, especially in the impacted zone, decreased TR in regions of elevated T2 as consistent with ischemia may reflect several pathophysiological processes including neurite beading and cell swelling. On the contrary, increased TR in gray matter regions of elevated T2 may indicate necrosis of the tissue, although this was unintended in the mild CCI model and not observed in histological observation. Taken together these observations underscore the utility of diffusion metrics to confer additional information about the pathological environment.

Although vascular pathology and ischemia are important contributing factors to the cellular alterations that evolve following TBI, they comprise only one facet of a complex response. Coordinated responses to trauma that may affect the microstructural environment include, among others, inflammation, neurite remodeling, and vulnerability of the myelinated axons in white matter. A number of diffusion MRI studies in rodents have identified astrocytic response to experimental TBI as an underlying factor for diffusion metric abnormalities following experimental injury (7, 13), and several studies have related changes to anisotropy metrics with damage to the myelin sheath and axonal pathology (6, 11). In the current study, we compared *ex vivo* DTI of three ferret brains with histological markers in the same tissue. We found a number of features demonstrable by immunohistochemistry, even at 1-day post-TBI, that corresponded with alterations in the MR images. One of the main findings was an alteration in microglial state and distribution, showing that these cells changed their morphology and became more reactive very quickly after injury. This demonstrates that microglia are highly capable of adapting to changes in their environment and altering their morphology and function to local demands. Importantly, our findings demonstrate that these changes are visible on MR images. The net indication from these observations is that although clear markers of neuronal and glial pathology are related to the DTI abnormalities present following CCI, it is unlikely that a one-to-one correspondence exists between the pathomechanisms of TBI and the imaging outcomes. Rather, it is a combination of cellular alterations that comprise the coordinate tissue response to brain injury and give rise to MRI markers.

CONCLUSIONS

This study provides an initial characterization of the quantitative MRI alterations that follow experimental brain injury in a recently developed ferret model of mild focal TBI. The imaging tools of T2 imaging and DTI that were implemented in this study seem to provide sensitive and complementary information about the pathophysiology and cellular alterations that emerge during the acute time period. Furthermore, the similarity of the imaging abnormalities in the ferret brain with what has been observed in human studies provides promising evidence that this model may help to advance the translational relevance for preclinical studies of TBI. Despite the promise of preclinical studies to have an impact on the diagnosis and treatment of patients, a path to clinical relevance remains elusive and has numerous hurdles that are evident in the limitations of the current study. For example, the ferret model of TBI is new and relatively uncharacterized in the field of adulthood neurological disorders, and the cost and care of ferrets preclude studies with sample sizes that are as large as for rodent studies. In addition, although imaging tools hold promise across human and animal studies, the existing tools may not be sensitive enough to detect posttraumatic changes in the brain especially following mild injury. Nevertheless, many avenues for future work can be envisioned including modification of the ferret model or imaging approaches to target particular gaps in knowledge about the pathology of brain injury as well as longitudinal consideration of other time periods following TBI. In particular, blast and closed head injury models, which are more similar than CCI to human injury, may be robust in the ferret. In addition, improvements in quantitative MRI methods including novel acquisition and modeling methods and statistical approaches for identifying single-subject abnormalities in the absence of a baseline scan may confer greater utility for future studies.

ACKNOWLEDGMENTS

The authors thank the Congressionally Directed Medical Research Programs (CDMRP) for funding this work (award numbers W81XWH-13-2-0019 and W81XWH-13-2-0018) and The Henry M. Jackson Foundation for the Advancement of Military Medicine, Inc (HJF) for administration. They also thank the Center for Neuroscience and Regenerative Medicine (CNRM) for core facility support enabling this work, especially the translational imaging facility, Asamoah Bosomtwi and Alexandru Korotcov for *in vivo* MRI support, and are also grateful to Miki Komlosh for her help developing *ex vivo* MRI acquisition methods.

REFERENCES

1. Duhaime A-CC, Gean AD, Haacke EM, Hicks R, Wintermark M, Mukherjee P, Brody D, Latour L, Riedy G, Members P: Common data elements in radiologic imaging of traumatic brain injury. *Arch Phys Med Rehabil* 91(11):1661–1666, 2010.
2. Haacke EM, Duhaime AC, Gean AD, Riedy G, Wintermark M, Mukherjee P, Brody DL, DeGraba T, Duncan TD, Elovic E, et al.: Common data elements in radiologic imaging of traumatic brain injury. *J Magn Reson Imaging* 32(3):516–543, 2010.
3. Riedy G, Senseney JS, Liu W, Ollinger J, Sham E, Krapiva P, Patel JB, Smith A, Yeh P-HH, Graner J, et al.: Findings from structural MR imaging in military traumatic brain injury. *Radiology* 279:207–215, 2016.

4. Hulkower MB, Poliak DB, Rosenbaum SB, Zimmerman ME, Lipton ML: A decade of DTI in traumatic brain injury: 10 years and 100 articles later. *AJNR Am J Neuroradiol* 34(11):2064–2074, 2013.
5. Immonen R, Heikkinen T, Tähtivaara L, Nurmi A, Stenius T-KK, Puoliväli J, Tuinstra T, Phinney AL, Van Vliet B, Yrjänheikki J, et al.: Cerebral blood volume alterations in the perilesional areas in the rat brain after traumatic brain injury–comparison with behavioral outcome. *J Cereb Blood Flow Metab* 30(7):1318–1328, 2010.
6. Bennett RE, Mac Donald CL, Brody DL: Diffusion tensor imaging detects axonal injury in a mouse model of repetitive closed-skull traumatic brain injury. *Neurosci Lett* 513(2):160–165, 2012.
7. Budde MD, Janes L, Gold E, Turtzo L, Frank JA: The contribution of gliosis to diffusion tensor anisotropy and tractography following traumatic brain injury: validation in the rat using Fourier analysis of stained tissue sections. *Brain* 134(pt 8):2248–2260, 2011.
8. Calabrese E, Du F, Garman RH, Johnson GA, Riccio C, Tong LC, Long JB: Diffusion tensor imaging reveals white matter injury in a rat model of repetitive blast-induced traumatic brain injury. *J Neurotrauma* 31(10):938–950, 2014.
9. Immonen RJ, Kharatishvili I, Gröhn H, Pitkänen A, Gröhn OH: Quantitative MRI predicts long-term structural and functional outcome after experimental traumatic brain injury. *NeuroImage* 45(1):1–9, 2009.
10. Long JA, Watts LT, Chemello J, Huang S, Shen Q, Duong TQ: Multiparametric and longitudinal MRI characterization of mild traumatic brain injury in rats. *J Neurotrauma* 32(8):598–607, 2015.
11. Mac Donald CL, Dikranian K, Song SK, Bayly PV, Holtzman DM, Brody DL: Detection of traumatic axonal injury with diffusion tensor imaging in a mouse model of traumatic brain injury. *Exp Neurol* 205(1):116–131, 2007.
12. Xu S, Zhuo J, Racz J, Shi D, Roys S, Fiskum G, Gullapalli R: Early microstructural and metabolic changes following controlled cortical impact injury in rat: a magnetic resonance imaging and spectroscopy study. *J Neurotrauma* 28(10):2091–2102, 2011.
13. Zhuo J, Xu S, Proctor JL, Mullins RJ, Simon JZ, Fiskum G, Gullapalli RP: Diffusion kurtosis as an in vivo imaging marker for reactive astrogliosis in traumatic brain injury. *NeuroImage* 59(1):467–477, 2012.
14. Schwerin S, Hutchinson E, Ngalula K, Pierpaoli C, Juliano S: Development of a ferret model of traumatic brain injury; preliminary imaging, behavioral and immunohistochemical findings. *Poster presented (22518/M8) at the 44th Annual Meeting of the Society for Neuroscience*; 2014. Washington, DC.
15. Irfanoglu MO, Modi P, Nayak A, Hutchinson EB, Sarlls J, Pierpaoli C: DR-BUDDI (Diffeomorphic Registration for Blip-Up blip-Down Diffusion Imaging) method for correcting echo planar imaging distortions. *NeuroImage* 106:284–299, 2015.
16. Pierpaoli C, Walker L, Irfanoglu M, Barnett A, Chang LC, Koay C, Pajevic S, Rohde G, Sarlls J, Wu M: TORTOISE: an integrated software package for processing of diffusion MRI data. *Poster presented at the ISMRM 19th Annual Meeting*; 2010. Stockholm, Sweden.
17. Pajevic S, Pierpaoli C: Color schemes to represent the orientation of anisotropic tissues from diffusion tensor data: application to white matter fiber tract mapping in the human brain. *Magn Reson Med* 42(3):526–540, 1999.
18. Irfanoglu MO, Nayak A, Jenkins J, Hutchinson EB, Sadeghi N, Thomas CP, Pierpaoli C: DR-TAMAS: Diffeomorphic Registration for Tensor Accurate Alignment of Anatomical Structures. *NeuroImage* 132:439–454, 2016.
19. Arfanakis K, Hermann BP, Rogers BP, Carew JD, Seidenberg M, Meyerand ME: Diffusion tensor MRI in temporal lobe epilepsy. *Magn Reson Imaging* 20(7):511–519, 2002.
20. Huisman TA, Schwamm LH, Schaefer PW, Koroshetz WJ, Shetty-Alva N, Ozsunar Y, Wu O, Sorensen AG: Diffusion tensor imaging as potential biomarker of white matter injury in diffuse axonal injury. *AJNR Am J Neuroradiol* 25(3):370–376, 2004.
21. Perez AM, Adler J, Kulkarni N, Strain JF, Womack KB, Diaz-Arrastia R, Marquez de la Plata CD: Longitudinal white matter changes after traumatic axonal injury. *J Neurotrauma* 31(17):1478–1485, 2014.
22. Sotak CH: The role of diffusion tensor imaging in the evaluation of ischemic brain injury—a review. *NMR Biomed* 15(7–8):561–569, 2002.
23. Pierpaoli C, Righini A, Linfante I, Tao-Cheng JH, Alger JR, Di Chiro G: Histopathologic correlates of abnormal water diffusion in cerebral ischemia: diffusion-weighted MR imaging and light and electron microscopic study. *Radiology* 189(2):439–448, 1993.